

Analyzing Rydberg excitation Dynamics in an atomic chain via discrete truncated Wigner approximation and artificial neural networks

Vighnesh Naik¹, Varna Shenoy¹, Weibin Li², and Rejish Nath¹

¹Department of Physics, Indian Institute of Science Education and Research Pune, Dr. Homi Bhabha Road, Pune- 411008, Maharashtra, India.

² School of Physics and Astronomy, and Centre for the Mathematics and Theoretical Physics of Quantum Non-Equilibrium Systems, University of Nottingham, NG7 2RD, United Kingdom.

Abstract. We analyze the excitation dynamics numerically in a one-dimensional Rydberg atomic chain, using the methods of discrete truncated Wigner approximation (dTWA) and artificial neural networks (ANN), for both van der Waals and dipolar interactions. In particular, we look at how the number of excitations dynamically grows or evolves in the system for an initial state where all atoms are in their electronic ground state. Further, we calculate the maximum number of excitations attained at any instant and the average number of excitations. For a small system size of ten atoms, we compare the results from DTWA and ANN with that of exact numerical calculations of the Schrödinger equation. The collapse and revival dynamics in the number of Rydberg excitations are also characterized in detail. Though we find good agreement at shorter periods, both DTWA and ANN failed to capture the dynamics quantitatively at longer times. By increasing the number of hidden units, the accuracy of ANN is significantly improved but suffered by numerical instabilities, especially for large interaction strengths. Finally, we look at the dynamics of a large system using dTWA.

Contents

1	Introduction	2
2	Setup and Model	4
3	Discrete truncated Wigner approximation	5
3.1	Phase space sampling schemes	7
4	Artificial neural networks: RBM machine	8
5	Dynamics in a small chain of $N = 10$: Comparison between exact, dTWA and ANN results	11
5.1	Single site dynamics	13
5.2	Long time dynamics in small chains: Collapse and revival	14
6	Large System dynamics	16
7	Conclusions and Outlook	17
8	Acknowledgments	18

1. Introduction

In general, analyzing the dynamics of a quantum many-body system is a formidable task, and the complexity increases with the system size. The latter is due to the exponentially growing Hilbert space with system size. Along with that, strong quantum correlations or entanglement growth makes quantum dynamics more intriguing. Developing numerical approaches capturing quantum correlations have been one of the main focus in the recent past [1], and lead to the development of various numerical techniques based on tensor network states and phase-space methods. The former includes, for instance, density-matrix renormalization group (DMRG) (for both ground states and dynamics) [2–7] in which the Hilbert space is truncated to states with significant probabilities, thereby leading to a polynomial growth in Hilbert space with system size. DMRG is found to be an excellent tool for studying one-dimensional systems with weak entanglement. On the other side, examples for the phase-space methods are truncated Wigner approximation (TWA) [8, 9] and its discrete version (dTWA) [10–12], which are semi-classical approaches involving classical equations of motion for the phase-space variables. Though initially dTWA was developed for coherent spin-1/2 systems, later generalized to higher spin systems [13], higher dimensional phase space [14] and dissipative systems [15]. dTWA is recently employed to study large spin systems in which dynamical phase transitions are explored [16]. Also, the results from dTWA are found to be in excellent agreement with experiments using Rydberg [17–20] and dipolar atoms [21–23]. The Rydberg experiments explored the magnetization relaxation dynamics in

a quantum spin system [17–19] and superradiance triggered by black-body radiation [20], in which the quantum fluctuations are accommodated in the sampling of the initial state. As discussed in [24], dTWA may breaks down at longer times depending on the system parameters, especially depending on the range of the interactions.

At the same time, there is a growing interest in using machine learning methods to study problems in physics [25, 26]. In particular, artificial neural networks (ANN) are proposed to study quantum many-body systems in which the quantum states are represented by restricted-Boltzmann-machine (RBM) type network structure with complex weights [27]. Due to its structure, RBM is naturally suited for spin-1/2 systems. The RBM ansatz is found to be capturing both ground states and quantum dynamics accurately for various quantum many-body models, including multi-dimensional systems [28, 29, 31, 32]. It is also proposed to find quantum nonlocality in many-body systems [33].

Recently, the experiments using Rydberg atoms have shown tremendous progress, extending the limit of quantum simulators to large system sizes beyond a regime where classical computers can solve [34–43]. Still, it is necessary to develop or test different numerical approaches to benchmark the physics of systems with small to moderate sizes. What makes Rydberg atoms special are their prodigious interactions [44, 45] that can suppress further excitations within a finite volume leading to the phenomenon of the Rydberg, or dipole blockade [46–48]. Blockade and anti-blockade become crucial mechanisms for applications from quantum many-body physics [35, 49–55] to quantum information protocols [44, 56–60]. Usually, the Rydberg setup has been modelled as a gas of interacting two-level atoms (qubits), with interactions of either dipolar or van der Waals type. Additional control over the quantum states of the system can be attained by introducing a time-dependence in the atom-field coupling parameters for instance, periodic driving [43, 61].

In this work, we numerically analyze the dynamics of Rydberg excitations in an atomic chain in which all atoms are initially prepared in the ground state, employing both dTWA and ANN (RBM network). We consider the cases of both van der Waals and dipolar interactions between the Rydberg atoms. In particular, we look at the growth of Rydberg excitations in the system as a function of interaction strengths. The number of excitations exhibits an oscillatory behaviour in time, and the system attains the maximum number of excitations in the first excitation cycle, irrespective of the nature of interactions. Both maximum and mean number of excitations in the system decrease with an increase in interaction strength due to the Rydberg blockade. For a small system size of ten atoms, we compare the long-time dynamics from dTWA and ANN with exact numerical results. At shorter times and for small interaction strengths, dTWA capture dynamics accurately, whereas it breaks down at longer times and for higher interactions strengths. The accuracy of the ANN results depends on the number of hidden units. Including multi-particle correlations via BBGKY hierarchy in dTWA and increasing the number of hidden units in ANN with large interaction strengths suffer numerical instabilities. The latter prevent us from exploring the long-time dynamics using ANN.

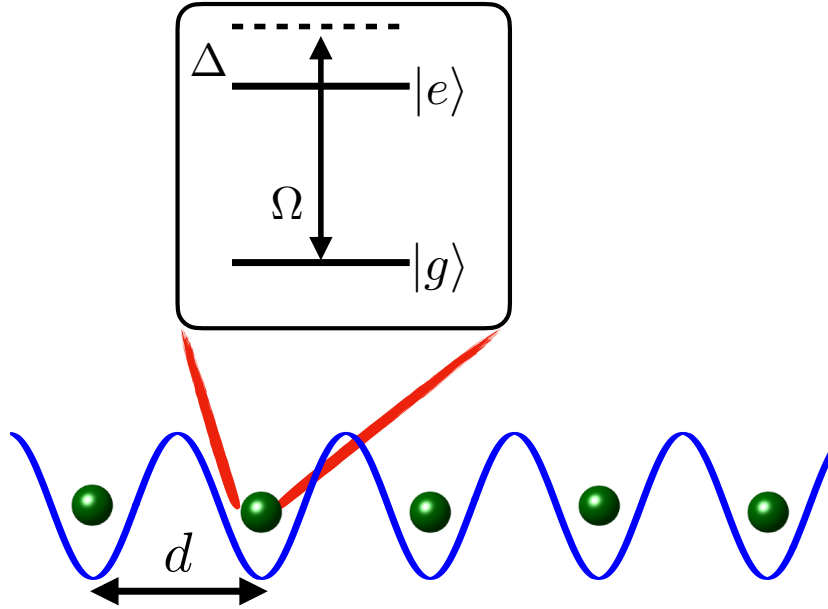


Figure 1. The schematic diagram of the setup we consider. In each atom, the ground state $|g\rangle$ is coupled to a Rydberg state $|e\rangle$ with a light field with a detuning Δ and Rabi frequency Ω .

An important feature in the dynamics, collapses and revivals are characterized in detail as function of interaction strength and atom-light detuning. Finally, we discuss the dynamics in a large system of two-hundred atoms using dTWA.

The paper is structured as follows. In section 2, we introduce the physical setup and the governing Hamiltonian. In section 3, we discuss the dTWA method and in section 3.1 we introduce the different sampling schemes used for representing the initial state. The ANN based on RBM is briefly discussed in section 4. The excitation dynamics in a small chain of 10 atoms are studied in section 5. The single site dynamics and the collapses and revivals of the number of excitations are discussed in sections 5.1 and 5.2, respectively. Finally, the dynamics in a system of $N = 200$ is studied using dTWA in section 6. We conclude in section 7.

2. Setup and Model

We consider a chain of atoms with lattice spacing d as shown in Figure 1. For each atom, the electronic ground state $|g\rangle$ is coupled to a Rydberg state $|e\rangle$ with a detuning Δ and a Rabi frequency Ω . In the frozen gas limit, the system is described by the Hamiltonian ($\hbar = 1$):

$$\hat{H}(t) = -\Delta \sum_{i=1}^N \hat{\sigma}_{ee}^i + \frac{\Omega}{2} \sum_{i=1}^N \hat{\sigma}_x^i + \sum_{i < j} V_{ij} \hat{\sigma}_{ee}^i \hat{\sigma}_{ee}^j, \quad (1)$$

where $\hat{\sigma}_{ab} = |a\rangle\langle b|$ with $a, b \in \{e, g\}$ includes both transition and projection operators, and $\hat{\sigma}_x = \hat{\sigma}_{eg} + \hat{\sigma}_{ge}$. We assume the Rydberg excited atoms interact via a potential

$V_{ij} = C_\alpha/r_{ij}^\alpha$ with $\alpha = 3$ (dipolar) and $\alpha = 6$ (van der Waals) [45], where C_α is the interaction coefficient, and r_{ij} is the separation between i th and j th Rydberg excitations. The dipole-dipole interactions ($\alpha = 3$) between the two Rydberg excitations can be realized using an external electric field [62]. The exact dynamics of the system is analyzed by solving the Schrödinger equation: $i\partial\psi(t)/\partial t = \hat{H}(t)\psi(t)$, which we then compare with the results obtained from dTWA and ANN for small system sizes. The dTWA and ANN methods are then used for obtaining the excitation dynamics in larger systems. For the convenience, we express the Hamiltonian as, $\hat{H} = \sum_i \hat{H}_i + \sum_{i < j} \hat{H}_{ij}$, where $\hat{H}_i = -\Delta_i^{\text{eff}}\hat{\sigma}_z^i + \Omega\hat{\sigma}_x^i/2$ is the single particle term with $\Delta_i^{\text{eff}} = \Delta - \sum_{j \neq i} V_{ij}/2$ and $\hat{H}_{ij} = V_{ij}\hat{\sigma}_z^i\hat{\sigma}_z^j/4$ is the interaction term. We have used $\hat{\sigma}_{ee}^i = (1 + \hat{\sigma}_z^i)/2$ for writing \hat{H}_i and \hat{H}_{ij} . For the dynamics we calculate the total number of excitations $N_e(t) = \sum_i \langle \hat{\sigma}_{ee} \rangle$ at any instant t , the maximum number of excitations N_e^{max} attained, and the average number of excitations $N_e^{\text{avg}} = (1/T) \int_0^T N_e(t) \text{d}t$ over a sufficiently long period of time T .

3. Discrete truncated Wigner approximation

In this section, we briefly outline the numerical method of dTWA. Each atom is seen as a two-level system (equivalently a qubit or a spin-1/2 particle) composed of the ground state $|g\rangle$ and Rydberg state $|e\rangle$, localized at a point in space. Thus, our setup is spanned by a finite and discrete Hilbert space, which has to be mapped onto a discrete quantum phase-space via Wigner-Weyl transform. A single qubit discrete phase-space is defined as a real-valued finite field spanned by four-phase points, denoted by $\alpha \equiv (m, n) \in \{(0, 0), (0, 1), (1, 0), (1, 1)\}$ [10, 63, 64]. For each phase-space point, one can associate a phase-point operator $\hat{A}_\alpha = (\mathcal{I} + \mathbf{r}_\alpha \cdot \hat{\sigma})/2$, where \mathcal{I} is the identity operator and $\hat{\sigma} = (\hat{\sigma}_x, \hat{\sigma}_y, \hat{\sigma}_z)$ are the Pauli matrices. The three-vectors $\{\mathbf{r}_\alpha\}$ do not have a unique choice, and the best suitable sampling scheme for a given Hamiltonian can be appropriately selected [12]. The commonly used five sampling schemes ($S_I - S_V$) are discussed in Section 3.1. For the Hamiltonian in equation (1), we found that the schemes S_{III} , S_{IV} and S_V are most suited, which is verified by comparing the dTWA results with the exact ones in a setup of $N = 10$, as discussed in Section 3.1.

Any observable \hat{O} from the Hilbert space is mapped into a Weyl symbol $\mathcal{O}_\alpha^W = \text{Tr}(\hat{O}\hat{A}_\alpha)/2$ in the discrete phase-space. The density operator $\hat{\rho}$ is written as $\hat{\rho} = \sum_\alpha w_\alpha \hat{A}_\alpha$, where the weights $w_\alpha = \text{Tr}(\hat{\rho}\hat{A}_\alpha)/2$ form a quasi-probability distribution similar to the original Wigner function for continuous degrees of freedom and is the Weyl symbol of the density matrix. w_α can also take negative values. Now, for a system of N Rydberg two-level atoms, we have a discrete phase-space of 4^N points denoted by $\alpha = \{\alpha_1, \alpha_2, \dots, \alpha_N\}$. Let the initial density matrix be,

$$\hat{\rho}_0 = \sum_\alpha W_\alpha \hat{A}_{\alpha_1} \otimes \hat{A}_{\alpha_2} \otimes \dots \otimes \hat{A}_{\alpha_N}, \quad (2)$$

which corresponds to a product state and we define $W_\alpha = w_{\alpha_1}w_{\alpha_2}\dots w_{\alpha_N}$. Then, the

density matrix at time t is provided by

$$\hat{\rho}(t) = \sum_{\alpha} W_{\alpha} \hat{\mathcal{A}}_{1\dots N}^{\alpha_1\dots\alpha_N}(t), \quad (3)$$

in which

$$\hat{\mathcal{A}}_{1\dots n}^{\alpha_1\dots\alpha_n}(t) = \hat{U}(t) \hat{A}_{\alpha_1} \otimes \hat{A}_{\alpha_2} \otimes \dots \otimes \hat{A}_{\alpha_N} \hat{U}^{\dagger}(t) \quad (4)$$

where $\hat{U}(t) = \exp(-i\hat{H}t)$ is the unitary time evolution operator. The operator $\hat{\mathcal{A}}_{1\dots N}^{\alpha_1\dots\alpha_N}(t)$ satisfies the Liouville-von Neumann equation [12]:

$$i \frac{\partial}{\partial t} \hat{\mathcal{A}}_{1\dots N}^{\alpha_1\dots\alpha_N} = [\hat{H}, \hat{\mathcal{A}}_{1\dots N}^{\alpha_1\dots\alpha_N}] \quad (5)$$

Treating the operator $\hat{\mathcal{A}}_{1\dots N}^{\alpha_1\dots\alpha_N}$ as a quasi-density-matrix since its trace is equal to one, but need not be positive definite, one can define reduced \hat{A} operators by tracing out some parts as follows:

$$\hat{A}_i^{\alpha_1\dots\alpha_N} = \text{Tr}_{\not{i}} \hat{\mathcal{A}}_{1\dots N}^{\alpha_1\dots\alpha_N}, \quad \hat{A}_{ij}^{\alpha_1\dots\alpha_N} = \text{Tr}_{\not{i}\not{j}} \hat{\mathcal{A}}_{1\dots N}^{\alpha_1\dots\alpha_N} \quad (6)$$

where $\text{Tr}_{\not{i}}$ denotes a partial trace over all the indices except i and similarly for $\text{Tr}_{\not{i}\not{j}}$ with $i \neq j$. For reduced density operators, using the Liouville-von Neumann equation, one can write down the hierarchy of equations of motions, so-called the BBGKY hierarchy. Following the same prescription, a similar hierarchy of equations of motions for the reduced \hat{A} operators is obtained, by introducing the cluster expansion [12],

$$\hat{A}_{ij} = \hat{A}_i \hat{A}_j + \hat{C}_{ij} \quad (7)$$

$$\hat{A}_{ijk} = \hat{A}_i \hat{A}_j \hat{A}_k + \hat{A}_i \hat{C}_{jk} + \hat{A}_j \hat{C}_{ik} + \dots + \hat{C}_{ijk} \quad (8)$$

$$\hat{A}_{ijkl} = \hat{A}_i \hat{A}_j \hat{A}_k \hat{A}_l + \hat{A}_i \hat{A}_j \hat{C}_{kl} + \dots + \hat{C}_{ijk} \hat{A}_l + \dots + \hat{C}_{ijkl} \quad (9)$$

where $\hat{A}_1, \hat{A}_2, \dots, \hat{A}_N$ are the uncorrelated parts of $\hat{\mathcal{A}}_{1\dots N}$, and the $\hat{C}_{ij}, \hat{C}_{ijk\dots}$ operators incorporate the correlations between the particles arising from the inter-particle interactions. Note that, we have removed the superscripts in \hat{A}_j for simplicity. Truncating beyond two-particle correlations, one obtains the first two equations of the BBGKY hierarchy as:

$$i \frac{\partial}{\partial t} \hat{A}_i = [\hat{H}_i, \hat{A}_i] + \sum_{k \neq i} \text{Tr}[\hat{H}_{ik}, \hat{C}_{ik} + \hat{A}_i \hat{A}_k] \quad (10)$$

$$\begin{aligned} i \frac{\partial}{\partial t} \hat{C}_{ij} = & [\hat{H}_i + \hat{H}_j + \hat{H}_{ij}^H + \hat{H}_{ji}^H, \hat{C}_{ij}] + [\hat{H}_{ij}, \hat{C}_{ij} + \hat{A}_i \hat{A}_j] + \\ & \sum_{k \neq i,j} \left(\text{Tr}_k[\hat{H}_{ik}, \hat{A}_i \hat{C}_{jk}] + \text{Tr}_k[\hat{H}_{jk}, \hat{A}_j \hat{C}_{ik}] \right) - \\ & \hat{A}_i \text{Tr}_i[\hat{H}_{ij}, \hat{C}_{ij} + \hat{A}_i \hat{A}_j] - \hat{A}_j \text{Tr}_j[\hat{H}_{ij}, \hat{C}_{ij} + \hat{A}_i \hat{A}_j] \end{aligned} \quad (11)$$

where \hat{H}_{ij}^H is a Hartree operator or Mean-field operator given by:

$$\hat{H}_{ij}^H = \sum_{k \neq i,j} \text{Tr}_k(\hat{H}_{ik} \hat{A}_k). \quad (12)$$

At this point, one expands \mathcal{A} and \mathcal{C} operators in the basis of Pauli spin matrices,

$$\hat{\mathcal{A}}_i = \frac{1}{2}(\mathcal{I} + \hat{a}_i \cdot \hat{\sigma}) \quad (13)$$

$$\hat{\mathcal{C}}_{ij} = \frac{1}{4} \sum_{\mu, \nu \in \{x, y, z\}} c_{ij}^{\mu\nu} \hat{\sigma}_\mu^i \hat{\sigma}_\nu^j, \quad (14)$$

for $i \neq j$. Finally, obtaining the dynamical equations for the coefficients a_i^μ and $c_{ij}^{\mu\nu}$, which are a set of $3N(N-1)/2$ coupled ordinary differential equations and take the following forms after using the Hamiltonian in Equation. (1),

$$\frac{1}{2} \dot{a}_i^\mu = \sum_{\gamma} \left[\frac{\Omega}{2} a_i^\gamma \varepsilon^{\mu x \gamma} - \frac{\Delta_i^{\text{eff}}}{2} a_i^\gamma \varepsilon^{\mu z \gamma} + (G_i^z a_i^\gamma + G_i^{z\gamma}) \varepsilon^{\mu z \gamma} \right] \quad (15)$$

$$\begin{aligned} \frac{1}{2} \dot{c}_{ij}^{\mu\nu} = & \sum_{\beta} \frac{V_{ij}}{4} (a_i^\beta \delta_{\nu z} - a_j^\beta \delta_{\mu z}) \varepsilon^{\mu\nu\beta} + \sum_{\delta} c_{ij}^{\delta\nu} \left[\frac{\Omega}{2} \varepsilon^{x\delta\mu} + \left(G_{ij}^z - \frac{\Delta_i^{\text{eff}}}{2} \right) \varepsilon^{z\delta\mu} \right] \\ & + \sum_{\gamma} c_{ij}^{\mu\gamma} \left[\frac{\Omega}{2} \varepsilon^{x\gamma\nu} + \left(G_{ij}^z - \frac{\Delta_j^{\text{eff}}}{2} \right) \varepsilon^{z\gamma\nu} \right] + \sum_{\gamma} [G_{ij}^{\nu z} a_i^\gamma \varepsilon^{z\gamma\mu} + G_{ji}^{\mu z} a_j^\gamma \varepsilon^{z\gamma\nu}] \\ & - \sum_{\gamma} \frac{V_{ij}}{4} [a_i^\mu (c_{ij}^{z\gamma} + a_i^z a_j^\gamma) \varepsilon^{z\gamma\nu} + a_j^\nu (c_{ij}^{\gamma z} + a_i^\gamma a_j^z) \varepsilon^{z\gamma\mu}] \end{aligned} \quad (16)$$

where ε is the Levi-Civita symbol, $\Delta_i^{\text{eff}} = \Delta - \sum_{j \neq i} V_{ij}/2$, $G_i^z = \sum_{k \neq i} V_{ik} a_k^z / 4$, $G_i^{z\gamma} = \sum_{k \neq i} V_{ik} c_{ki}^{z\gamma} / 4$, $G_{ij}^z = \sum_{k \neq i, j} V_{ik} a_k^z / 4$, and $G_{ij}^{\nu z} = \sum_{k \neq i, j} V_{ik} c_{jk}^{\nu z} / 4$. Equations (15) and (16) describe the dynamics in a Rydberg atomic chain incorporating the two-body correlations. Note that the effect of interatomic interactions enter through the terms G_i^z in equation 15. For solving equations (15) and (16) we use a package RK45 from NumPy (Python), which employs fifth order Runge-Kutta formula. When the two-particle correlations from equation (16) are incorporated in the dynamics, we are suffered by numerical instabilities after a short period of time and therefore exclude from further discussions, i.e., we take $c_{ij}^{\mu\nu} = 0$. Thus, we solve $3N$ coupled first order differential equations for the dynamics. Once we obtain a_i^μ , we can calculate the expectation value of a single particle operator as,

$$\langle \hat{\sigma}_\mu^i \rangle(t) = \text{Tr} (\hat{\sigma}_\mu^i \hat{\rho}(t)) = \sum_{\alpha} W_\alpha \text{Tr} (\hat{\sigma}_\mu^i \hat{A}_{1 \dots N}^{\alpha_1 \dots \alpha_N}(t)) = \sum_{\alpha} W_\alpha a_i^\mu(t), \quad (17)$$

in which the total number of excitations $N_e(t)$ is related to $\langle \sigma_\mu^i \rangle(t)$ or equivalently $a_i^z(t)$.

3.1. Phase space sampling schemes

Here, we provide the different sampling schemes for describing the initial density matrix given in equation (2) [12]. In Section 5, we choose the most suitable sampling scheme for the model in equation (1) by studying the dynamics in an atom chain with $N = 10$, and comparing it with the exact numerical results. As mentioned before, the sampling schemes provided by $\{\mathbf{r}_\alpha\}$ defines the phase space operators, $\hat{A}_\alpha = (\mathcal{I} + \mathbf{r}_\alpha \cdot \hat{\sigma})/2$. Since the transformed operators, $\hat{A}'_\alpha = \hat{U} \hat{A}_\alpha \hat{U}^\dagger$ under a unitary transformation, also possesses the desired properties of a Wigner representation, and writing $\hat{A}'_\alpha = (\mathcal{I} + \mathbf{r}'_\alpha \cdot \hat{\sigma})/2$ we

identify new sampling scheme provided by $\{\mathbf{r}'_\alpha\}$ by a nonsingular linear transformation of the phase space coordinates [63]. Below, we consider the following sampling schemes:

Scheme 1 (S_I): This sampling scheme is based on Wootters's phase-space representation [63, 64]. Here, the phase-point operators are defined via the three vectors: $\mathbf{r}_{(0,0)} = (1, 1, 1)$, $\mathbf{r}_{(0,1)} = (-1, -1, 1)$, $\mathbf{r}_{(1,0)} = (1, -1, -1)$ and $\mathbf{r}_{(1,1)} = (-1, 1, -1)$.

Scheme 2 (S_{II}): This sampling scheme is obtained from the above sampling scheme, where the second component of each of the three vectors is flipped and we have $\mathbf{r}'_{(0,0)} = (1, -1, 1)$, $\mathbf{r}'_{(0,1)} = (-1, 1, 1)$, $\mathbf{r}'_{(1,0)} = (1, 1, -1)$ and $\mathbf{r}'_{(1,1)} = (-1, -1, -1)$.

Scheme 3 (S_{III}): A more general scheme can be chosen by combining two different phase space representations. Even though it goes beyond the original Wootters's discrete Wigner representation, the results found to be more closer to the exact ones as we will see later. The basic notion is that the initial density matrix can be divided into two parts, and use two different Wigner representations to describe the two halves. For instance, an initial density matrix for a spin, $\hat{\rho}_0 = (1 + \hat{\sigma}_z)/2$ can be represented by the vectors $\{\mathbf{r}_{(0,0)}, \mathbf{r}_{(0,1)}, \mathbf{r}'_{(0,0)}, \mathbf{r}'_{(0,1)}\}$. Similarly, to represent $\hat{\rho}_0 = (1 - \hat{\sigma}_z)/2$, one can choose $\{\mathbf{r}_{(1,0)}, \mathbf{r}_{(1,1)}, \mathbf{r}'_{(1,0)}, \mathbf{r}'_{(1,1)}\}$.

Scheme 4 (S_{IV}): This scheme is linear combination of \mathbf{r}_α and \mathbf{r}'_α , which takes the form: $\tilde{\mathbf{r}}_{(0,0)} = (1, 0, 1)$, $\tilde{\mathbf{r}}_{(0,1)} = (-1, 0, 1)$, $\tilde{\mathbf{r}}_{(1,0)} = (1, 0, -1)$ and $\tilde{\mathbf{r}}_{(1,1)} = (-1, 0, -1)$. Since $\tilde{\mathbf{r}}_\alpha$ does not include the fluctuations in the y -component, we can add that by introducing the additional three vectors, $\tilde{\mathbf{r}}'_{(0,0)} = (0, 1, 1)$, $\tilde{\mathbf{r}}'_{(0,1)} = (0, -1, 1)$, $\tilde{\mathbf{r}}'_{(1,0)} = (0, 1, -1)$ and $\tilde{\mathbf{r}}'_{(1,1)} = (0, -1, -1)$. Then, if the initial state is $\hat{\rho}_0 = (1 + \hat{\sigma}_z)/2$, we choose the vectors $\{(1, 0, 1), (-1, 0, 1), (0, 1, 1), (0, -1, 1)\}$, and if the initial state is $\hat{\rho}_0 = (1 - \hat{\sigma}_z)/2$, we consider the set $\{(1, 0, -1), (-1, 0, -1), (0, 1, -1), (0, -1, -1)\}$.

Scheme 5 (S_V): Here, we take the union of scheme 3 and 4 to get a new sampling sampling scheme. In this scheme, for the initial state $\hat{\rho}_0 = (1 + \sigma_z)/2$, we use the vectors $\{(1, 1, 1), (-1, -1, 1), (1, -1, 1), (-1, 1, 1), (1, 0, 1), (-1, 0, 1), (0, 1, 1), (0, -1, 1)\}$ and for the initial state $\hat{\rho}_0 = (1 - \sigma_z)/2$, we use the set $\{(1, -1, -1), (-1, 1, -1), (1, 1, -1), (-1, -1, -1), (1, 0, -1), (-1, 0, -1), (0, 1, -1), (0, -1, -1)\}$.

4. Artificial neural networks: RBM machine

In this section, we briefly describe the ANN method based on the RBM architecture, in which the network is schematically shown in figure 2 [27–29, 31–33]. In the RBM representation, the physical spins (neurons) $s_i \in \{1, -1\}$ in the primary layer are complemented by auxiliary layer of Ising spins (neurons) $h_j \in \{1, -1\}$. Each node in the primary layer is connected to each node in the auxiliary layer. There are no connections between nodes within a layer. The connection between s_i and h_j has a weight w_{ij} which is ij^{th} element of the weight matrix \mathbf{W} . RBM has bias weights a_i for the visible units and b_j for the hidden units with $i = 1, \dots, N$ and $j = 1, \dots, M$ and we take $M = \gamma N$, where we consider either $\gamma = 1$ or $\gamma = 4$. Larger the number of hidden units (γ), one would expect the results to be more accurate. In figure 2, we have shown an RBM for $N = 8$ and $\gamma = 2$. Now, the neural many-body quantum state (unnormalized) is defined

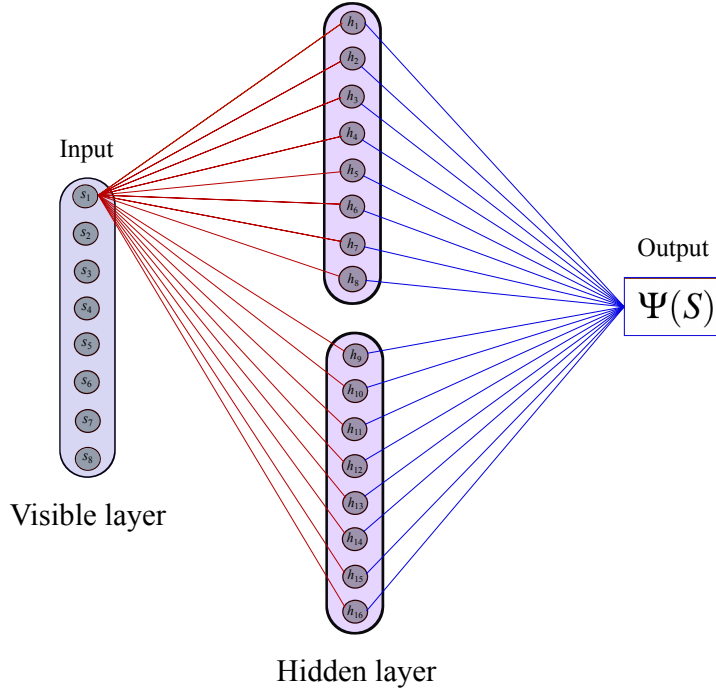


Figure 2. The schematic diagram for the ANN for system size of $N = 8$ and $M = 16$ i.e., for $\gamma = 2$. Each of the physical spin s_i connected to every hidden spin h_i (we have shown here only for one physical spin for clarity). The final output is the probability amplitude $\Psi(S)$ for a given spin configuration S .

as,

$$\Psi(S) = \sum_{\{h\}} \exp \left(\sum_i a_i s_i + \sum_j b_j h_j + \sum_i \sum_j s_i w_{ij} h_j \right), \quad (18)$$

where $S = (s_1, \dots, s_N)$ represents a spin configuration. We use $\hat{\sigma}_y$ basis to represent the spin configurations to obtain the correct results. $\Psi(S)$ determines the probability amplitude to find the particular spin configuration S . The first summation in equation (18) is over all the hidden spin configurations. By summing over the hidden units, we can write NQS in a compact form as

$$\Psi(S) = e^{\sum_i a_i s_i} \prod_{j=1}^M 2 \cosh \left(b_j + \sum_i w_{ij} s_i \right). \quad (19)$$

Note that we need to obtain the parameters w_{ij} , a_i and b_j for the initial state in which all atoms are in the electronic ground state. Typically, one obtains the initial state as the ground state of the Hamiltonian for carefully chosen set of parameters, via variational principle. The latter is interpreted as reinforcement learning of the ANN and is accomplished by means of a stochastic reconfiguration procedure [65, 66]. In our case, it is easy to estimate the initial state parameters in the $\hat{\sigma}_y$ basis and are $a_i = -i\pi/2$, $b_j = i\pi/4$, $w_{ij} = 0$. For the dynamics, we use the time-dependent variational principle,

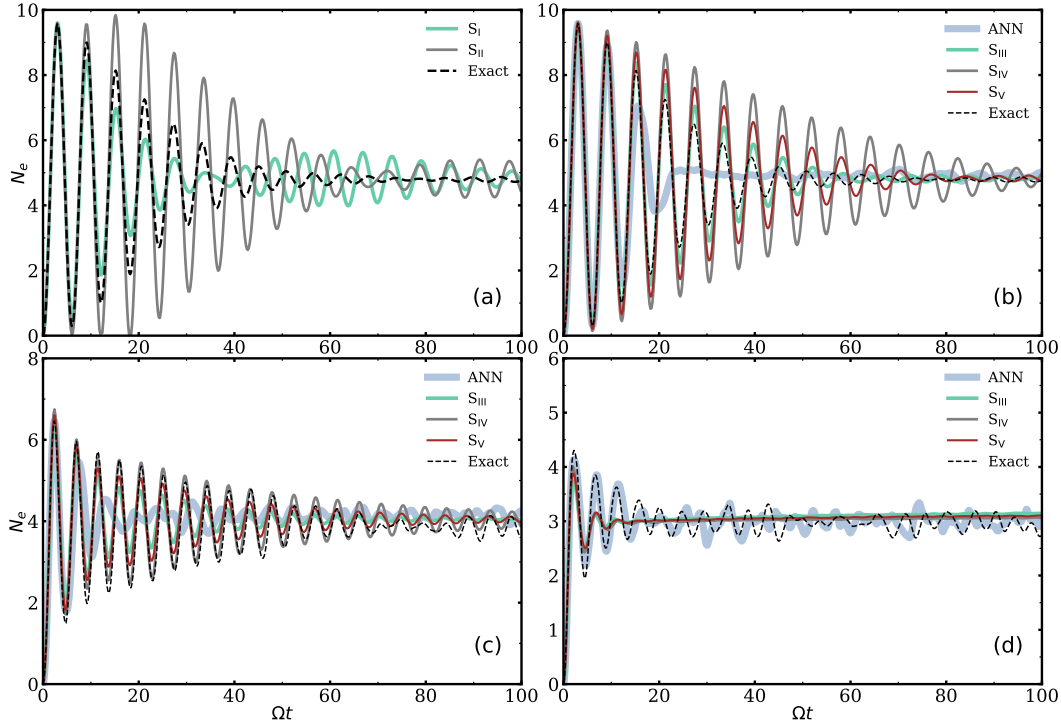


Figure 3. The dynamics of total number of excitations N_e in an atomic chain with $N = 10$, $\Delta = 0$ and for different C_6/d^6 . We compare the exact results (dashed line) with that from dTWA with different sampling schemes (thin lines) and ANN (thick line). In (a), we show the results for $C_6/d^6 = 0.2\Omega$ using S_I and S_{II} for dTWA, whereas in (b) we show the results using S_{III} , S_{IV} and S_V . In (c) and (d), we show the dynamics of $N_e(t)$ for $C_6/d^6 = \Omega$ and $C_6/d^6 = 3\Omega$, respectively, in which the exact results are compared with those obtained from the schemes S_{III} , S_{IV} and S_V for dTWA. For ANN, we took $N = M$, i.e., $\gamma = 1$.

which transforms the time-dependent Schrödinger equation into a non-linear set of symplectic differential equations for the variational parameters $\{w_{ij}, a_i, b_j\}$,

$$\dot{\mathbf{x}}(t) = -i\mathbf{S}^{-1}\mathbf{F}, \quad (20)$$

where \mathbf{x} is composed of the variational parameters, \mathbf{S} is a covariance matrix, and \mathbf{F} is generalized force. The elements of the matrix \mathbf{S} and the vector \mathbf{F} are

$$\mathbf{S}_{kk'} = \langle O_k^* O_{k'} \rangle - \langle O_k^* \rangle \langle O_{k'} \rangle \quad (21)$$

$$\mathbf{F}_k = \langle O_k^* E_{\text{loc}} \rangle - \langle O_k^* \rangle \langle E_{\text{loc}} \rangle, \quad (22)$$

where $\langle \dots \rangle$ is taken over $\Psi(S)$, and $O_{k'}^*(S)$ and $O_k(S)$ are variational derivatives given by

$$O_k(S) = \frac{1}{\Psi(S)} \frac{\partial \Psi(S)}{\partial x_k} \quad (23)$$

with E_{loc} being called the local energy, defined as

$$E_{\text{loc}}(S) = \frac{\langle S | \hat{H} | \Psi \rangle}{\langle S | \Psi \rangle}. \quad (24)$$

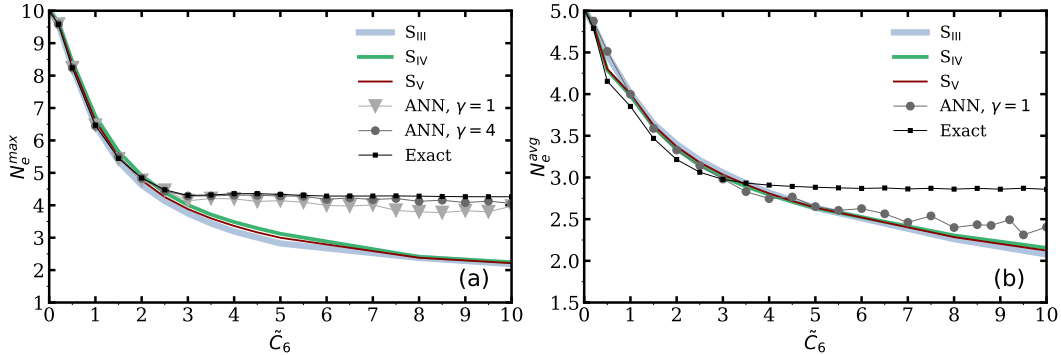


Figure 4. (a) The maximum (N_e^{max}) and (b) average (N_e^{avg}) number of excitations as a function of \tilde{C}_6 for $N = 10$ and $\Delta = 0$. We compare the exact results with that of DTWA and ANN. For calculating N_e^{avg} , we took $\Omega T = 45$ for ANN and $\Omega T = 100$ for dTWA and exact results. In (a) we show the results of ANN with both $\gamma = 1$ ($M = 10$) and $\gamma = 4$ ($M = 40$) and in (b) we show only for $\gamma = 1$ ($M = 10$).

When $\hat{\sigma}_z$ basis is used, $\mathbf{S}(t = 0)$ becomes a null matrix, and the system of equations does not evolve in time. One can either use the eigenstates of $\hat{\sigma}_x$ or $\hat{\sigma}_y$ basis to capture the dynamics and we use $\hat{\sigma}_y$ basis. We find that the results obtained by solving equation (20) using the Euler method and fourth-order Runge-Kutta (RK4) give us quantitatively identical results. We use the Euler method, as the RK4 becomes more time-consuming. The latter is because the \mathbf{S} matrix has a dimension of $(N+M+N \times M) \times (N+M+N \times M)$, and is constructed only once for each time step in Euler's method, whereas it is evaluated four times in the RK4 process. In any case, both approaches are suffered from numerical instabilities at a larger time [67]. Larger the value of α and the interaction strengths, the instability occurs earlier. For more details of the ANN approach, see [1, 27].

5. Dynamics in a small chain of $N = 10$: Comparison between exact, dTWA and ANN results

This section analyses the dynamics in a small system of $N = 10$ and compares the results from different methods. We take the initial state to be all atoms in the ground state $|g\rangle$ and calculate the total number of excitations (N_e) in the chain as a function of time. Figure 3 shows the dynamics of $N_e(t)$ for $\Delta = 0$ and different values of $\tilde{C}_6 = C_6/d^6$. For dTWA, we use different sampling schemes discussed in section 3.1 to represent the initial state and compare their results. At $t = 0$, we have $N_e = 0$, and as time evolves N_e increases and eventually oscillates in time. In the exact dynamics, the oscillation amplitude is larger at the first cycle, and it damps over the subsequent cycles. For sufficiently small values of C_6 and at longer times, we observe collapses and revivals in $N_e(t)$ about its average value [68], which we discuss in Section 5.2. Both the maximum number of excitations N_e^{max} [at the first peak of $N_e(t)$] and the average of number of excitations N_e^{avg} depend on the interaction strength \tilde{C}_6 and in particular, both N_e^{max} and N_e^{avg} decreases with increase in \tilde{C}_6 [see figure 4]. For $\tilde{C}_6 \ll \Omega$, we have $N_e^{max} \sim N$ and

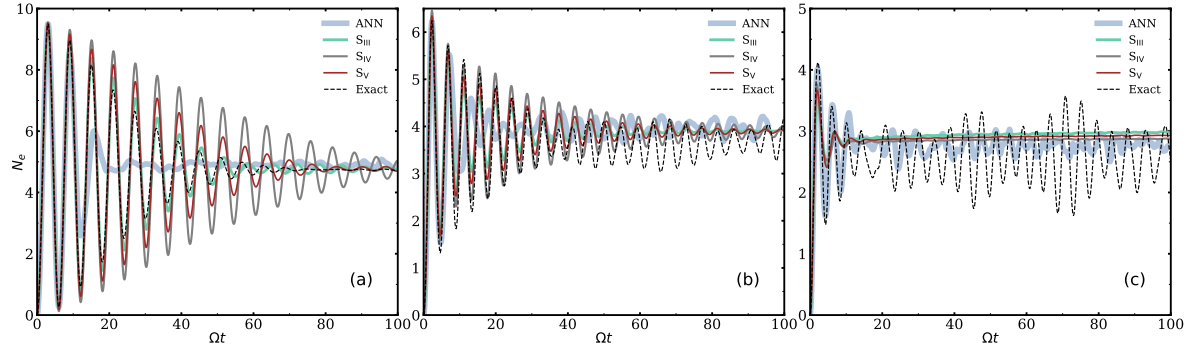


Figure 5. The dynamics of total number of excitations N_e in a periodic atomic chain with $N = 10$, $\Delta = 0$ and for different \tilde{C}_3 . We compare the exact results (dashed line) with that from dTWA with different sampling schemes (thin lines) and ANN (thick line). For dTWA we used the sampling schemes S_{III} , S_{IV} and S_{V} and or ANN, we took $N = M$, i.e., $\gamma = 1$. (a), (b) and (c) are respectively for $\tilde{C}_3 = 0.2\Omega$, $\tilde{C}_3 = \Omega$ and $\tilde{C}_3 = 3\Omega$. For ANN, we took $N = M$, i.e., $\gamma = 1$.

$N_e^{\text{avg}} \sim N/2$ and in a fully blockaded chain (limit $\tilde{C}_6 \rightarrow \infty$) $N_e^{\text{max}} \rightarrow 1$ and $N_e^{\text{avg}} \rightarrow 1/2$.

In the case of dTWA, we see that the results using the sampling schemes S_{III} , S_{IV} and S_{V} [see Figure 3(b)] are in better agreement with the exact results than those obtained using S_{I} and S_{II} [see Figure 3(a)]. Henceforth, we only use the schemes S_{III} , S_{IV} and S_{V} . Note that the instants of both maxima and minima are well captured by dTWA for small values of \tilde{C}_6 and showing a better agreement when $\tilde{C}_6 = \Omega$ [see Figure 3(c)]. The amplitude of the oscillations from dTWA is found to be larger than that of the exact results when \tilde{C}_6 is sufficiently small [see Figure 3(b) for $\tilde{C}_6 = 0.2\Omega$], whereas for large \tilde{C}_6 the amplitude decays to zero rather quickly in the dTWA results [see Figure 3(d) for $\tilde{C}_6 = 3\Omega$]. For large interaction strengths, both N_e^{max} and the amplitude of oscillations in $N_e(t)$ are smaller due to the Rydberg blockade. We also notice that for sufficiently large \tilde{C}_6 , the results using different sampling schemes become identical. In figures 3(b)-3(d), we also show ANN results using $\gamma = 1$, i.e., for $N = M = 10$. Since the system size is small, we were able to incorporate all possible spin configurations S in the calculation. For $\gamma > 1$, we are unable to capture the dynamics at longer times due to numerical instabilities. Larger the value of \tilde{C}_6 and α earlier the instability appears. Even for $\gamma = 1$, we see excellent agreement with the exact dynamics at shorter periods of time, irrespective of the value of \tilde{C}_6 . At longer times, the results from ANN with $\gamma = 1$ deviate from the exact dynamics but shows a better agreement than dTWA for large \tilde{C}_6 , in particular, the oscillations in $N_e(t)$ survive for large \tilde{C}_6 .

In figures 4(a) and 4(b), we show N_e^{max} and N_e^{avg} , respectively as a function of \tilde{C}_6 . For small values of \tilde{C}_6 , both ANN and dTWA are in good agreement with the exact results. Even though $N_e(t)$ exhibits a scheme dependent dynamics for dTWA, both N_e^{max} and N_e^{avg} are found to be scheme independent. We see that dTWA deviates significantly from the exact results for large \tilde{C}_6 and also exhibits a stronger blockade (smaller N_e^{max} and N_e^{avg}) than the actual ones. It indicates that the role of many-

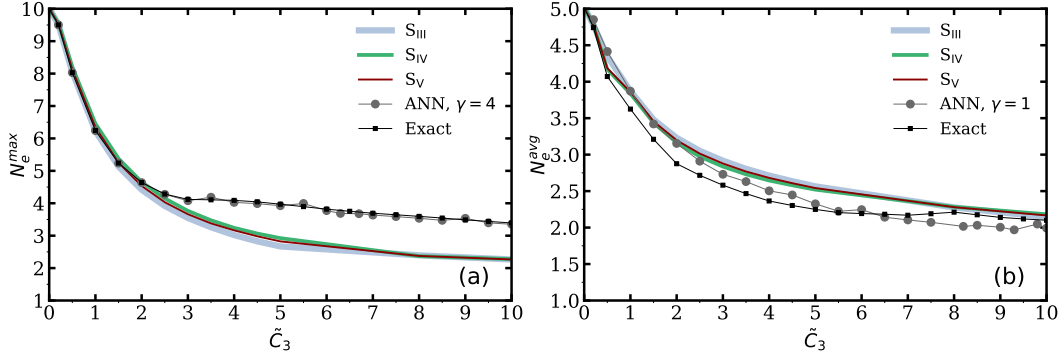


Figure 6. (a) The maximum (N_e^{max}) and (b) average (N_e^{avg}) number of excitations as a function of \tilde{C}_3 for $N = 10$ and $\Delta = 0$. We compare the exact results with that of dTWA in which we used the sampling schemes S_{III} , S_{IV} and S_{V} . For calculating N_e^{avg} , we took $\Omega T = 45$ for ANN and $\Omega T = 100$ for dTWA and exact results. In (a) we show the results of ANN with $\gamma = 4$ ($M = 40$) and in (b) we show for $\gamma = 1$ ($M = 10$).

body correlations in equation 16 is to enhance the Rydberg excitation population in the system. Since N_e^{max} [see figure 4(a)] is evaluated at the first excitation cycle, we are able to use ANN with $\gamma = 4$ without worrying about the numerical instability, which shows an excellent agreement with the exact results even at large \tilde{C}_6 . For comparison we also show the results using $\gamma = 1$, which exhibits some deviation from exact results but less than that of dTWA. On the other hand, to estimate N_e^{avg} , we require long time dynamics, which is possible only for ANN with $\gamma = 1$ [see figure 4(b)]. As we know ANN with $\gamma = 1$ is less accurate, especially at large interaction strengths which is visible in figure 4. For $3\Omega < \tilde{C}_6 \leq 10\Omega$, both N_e^{max} and N_e^{avg} saturate because the system exhibits nearest neighbour blockade (becomes effective for $\tilde{C}_6 > \Omega$), but the next nearest neighbour blockade requires an interaction strength of $\tilde{C}_6 \sim 64\Omega$. Thus, for larger and larger \tilde{C}_6 , one expects different low plateaus in N_e^{max} and N_e^{avg} vs \tilde{C}_6 indicating the blockades of nearest neighbour atoms and so on.

We find similar dynamics for the dipolar case as well, and the results are shown in figures 5 and 6. At longer times both ANN and dTWA results start to deviate from the exact results, as was in the case of van der Waals case. Also, for large \tilde{C}_3 , we do not see oscillations in $N_e(t)$ at longer times [see figure 5(c)]. For $\tilde{C}_6 = \tilde{C}_3 = 3\Omega$, the exact results show larger amplitude of oscillations for the dipolar case than the van der Waals case. In Figure 6, we show N_e^{max} and N_e^{avg} as a function of \tilde{C}_3 . Contrary to the van der Waals case, for dipolar case, dTWA gives a higher N_e^{avg} large interaction strengths compared to exact values [see Figure 6(b)]. For ANN, we use $\gamma = 4$ to estimate N_e^{max} and $\gamma = 1$ for N_e^{avg} and are in good agreement with the exact results for both.

5.1. Single site dynamics

In figure 7, we show the population dynamics in each site [$P_i(t)$] from both exact numerical calculations (upper row) and dTWA (lower row) for $N = 10$, $\Delta_0 = 0$ and

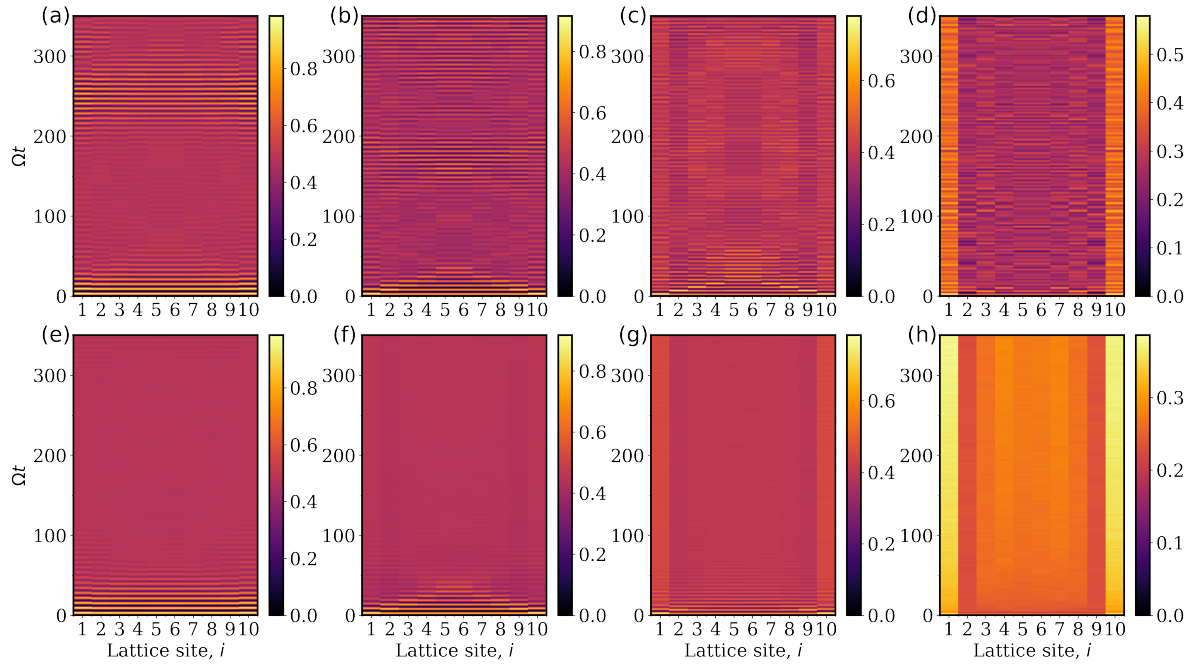


Figure 7. The dynamics of excitation probability in each site $P_i(t)$ in an atomic chain with $N = 10$, $\Delta = 0$ and (a) $\tilde{C}_6 = 0.1\Omega$, (b) $\tilde{C}_6 = 0.2\Omega$, (c) $\tilde{C}_6 = \Omega$, and (d) $\tilde{C}_6 = 5\Omega$. The corresponding results from DTWA using the sampling scheme S_{III} are shown in (e)-(h). Each column has same \tilde{C}_6 .

$\tilde{C}_6/\Omega = 0.2, 0.5, 1$ and 5 . For small interaction strengths ($\tilde{C}_6 \ll \Omega$), the population dynamics in every site is almost the same, similar to the non-interacting case. As the interaction strength increases, interaction dependent level shifts in various many-body configurations results in site-dependent dynamics [see figures 7(b)-7(d) and figures 7(f)-7(h)]. The latter becomes more apparent at large \tilde{C}_6 for which the Rydberg blockade prevents simultaneous excitation in the neighbouring sites and the distance between the excited atoms increases. For a sufficiently large interaction strength ($\tilde{C}_6 = 5\Omega$), it is more favourable to find the excitations at the edges of the lattice for $N = 10$ [see Figure 7(d)]. Though the dTWA results capture the general features, they differ from exact results, especially at longer times. For instance, in dTWA results, we do not observe local dynamics for sufficiently large interactions after the initial excitation cycles [see figures 7(g)-7(h)]. In the exact dynamics, the system never equilibrates and exhibits small amplitude oscillations.

5.2. Long time dynamics in small chains: Collapse and revival

As we mentioned in the previous section, $N_e(t)$ exhibits partial revivals and collapses at longer times for small values of interaction strengths [68]. The collapse and revival of $N_e(t)$ is identical to that of the population dynamics of a two-level atom coupled to a single-mode quantized light field in an optical cavity. In the latter case, the system is described by the well-known Jaynes-Cummings model (JCM). The collapse and revival

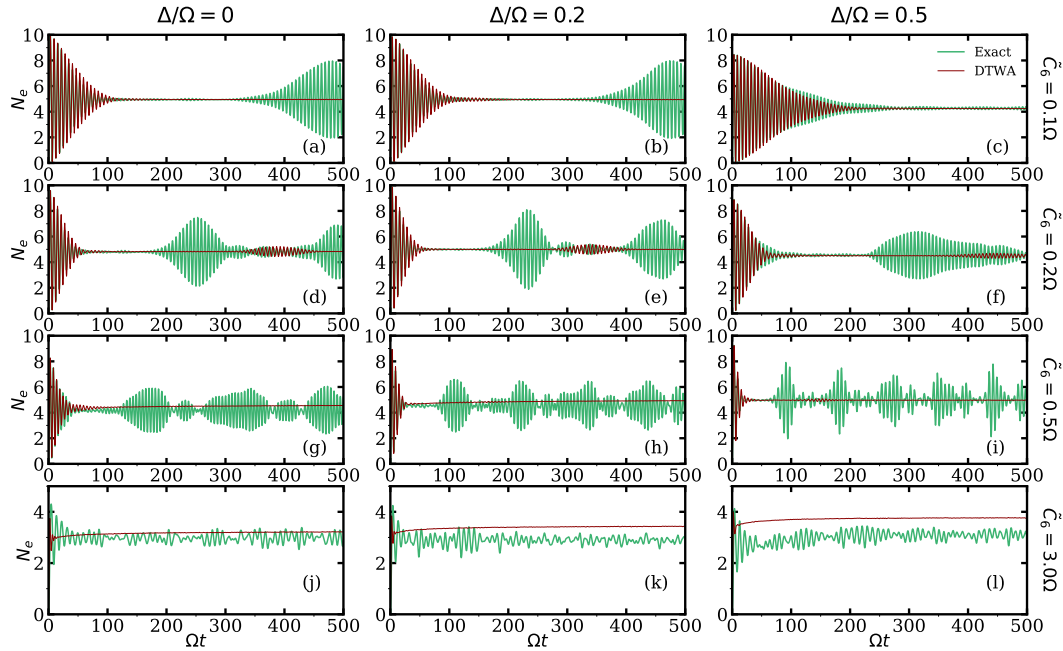


Figure 8. The long-time dynamics of total number of excitations N_e in an atomic chain with $N = 10$, for different \tilde{C}_6 and Δ . We compare the exact results with that from dTWA using the sampling schemes S_{III} .

in JCM are associated with the statistical and discrete nature of the photon field [69, 70]. In contrast, in the Rydberg chain, the collapse and revival in $N_e(t)$ can be attributed to the discrete nature of the physical setup.

Since similar results are seen for both dipolar and van der Waals cases, we only discuss the latter. In Figure 8, we show the dynamics of $N_e(t)$ for small values of Δ and \tilde{C}_6 . In general, the profile of the first collapse resembles a half-Gaussian in shape. Increasing the interaction strength \tilde{C}_6 has two effects (along the columns in figure 8): first, the collapse and revival duration reduce, and more non-trivial patterns arise in the population dynamics. Second, the amplitude of revivals decreases (see along the columns). In the exact dynamics, for sufficiently large \tilde{C}_6 , the revival disappears [see figures 8(j)-8(l)] and can be due to the Rydberg blockade. The results from dTWA shows no revival even for small values of \tilde{C}_6 [see figures 8(g)-8(i)]. Also, the collapse and revival dynamics depends nontrivially on the detuning Δ [see along the rows in figure 8]. For some values of Δ_0 and \tilde{C}_6 , the results from dTWA shown partial revivals (2nd row of Figure 8), but with lesser amplitudes than the exact dynamics. Due to the numerical instabilities occurring at longer times, we cannot simulate the revival features in the dynamics using ANN, even for $\gamma = 1$.

In Figure 9, we show long-time dynamics of $N_e(t)$ for $\tilde{C}_6 = 0.2\Omega$, $\Delta_0 = 0$ and different $N \in \{4, 10, 14\}$. In all cases, we see a sequence of collapses and revivals, with its frequency larger for $N = 4$. As N increases the initial collapsing period increases, which can also explain why in the classical limit $N \rightarrow \infty$, the revival disappears. For any N , the Gaussian envelope and the duration of the first collapse are maintained. At

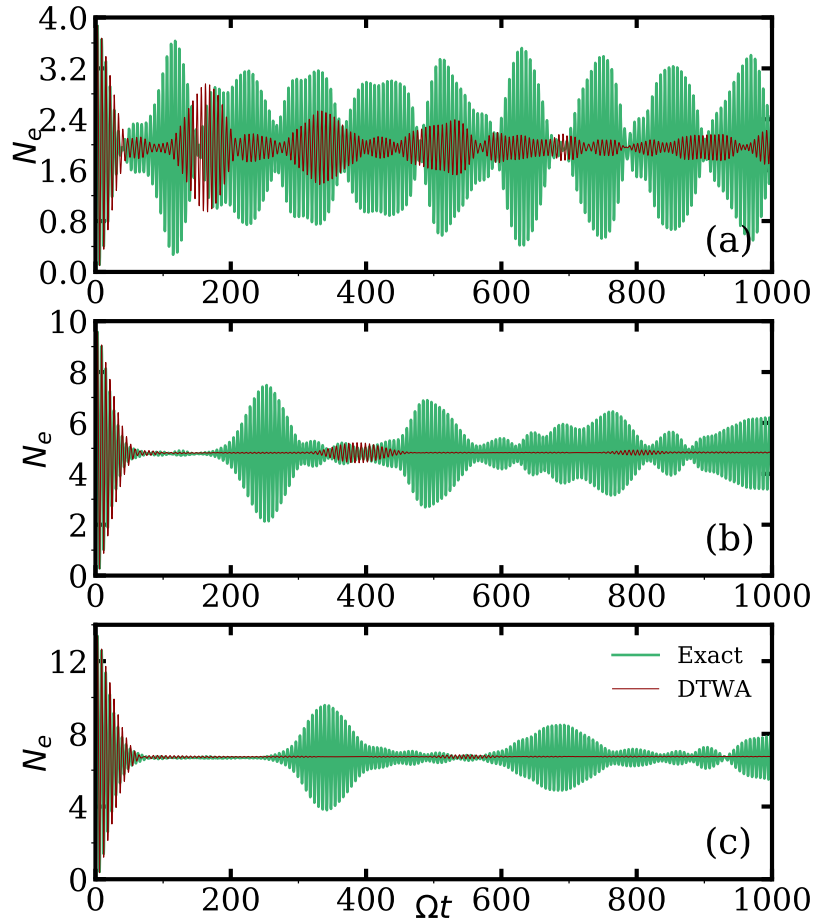


Figure 9. The long time dynamics of total number of excitations [$N_e(t)$] in a periodic atomic chain with (a) $N = 4$, (b) $N = 8$, (c) $N = 14$, and $\Delta = 0$, $C_6/d^6 = 0.2\Omega$. We compare the exact results with that from dTWA using the sampling schemes S_{III}.

a later time, $N_e(t)$ exhibits oscillation patterns which depends explicitly on N . As it was before, dTWA failed to capture the exact dynamics at longer periods of time, and hardly any revival is seen for $N = 14$ in the dTWA results [see Figure 9(c)].

6. Large System dynamics

Ultimately, we would like to simulate the dynamics in large systems. As we mentioned before, the Hilbert space of the system grows exponentially with the systems size N , which adds a limitation to the exact numerical calculations that we can do. It is extremely time consuming to analyze the long-time dynamics even for $N \sim 20$ taking into account of the full Hilbert space. In dTWA we have to only deal with $3N$ variable neglecting the correlations from equation 16, which helps us to simulate large system dynamics. As an example we show the excitation dynamics in a chain of $N = 200$, see figure 10 for both van der Waals and dipolar interactions. Both cases give us almost identical dynamics and as in the case of $N = 10$, the oscillations at longer

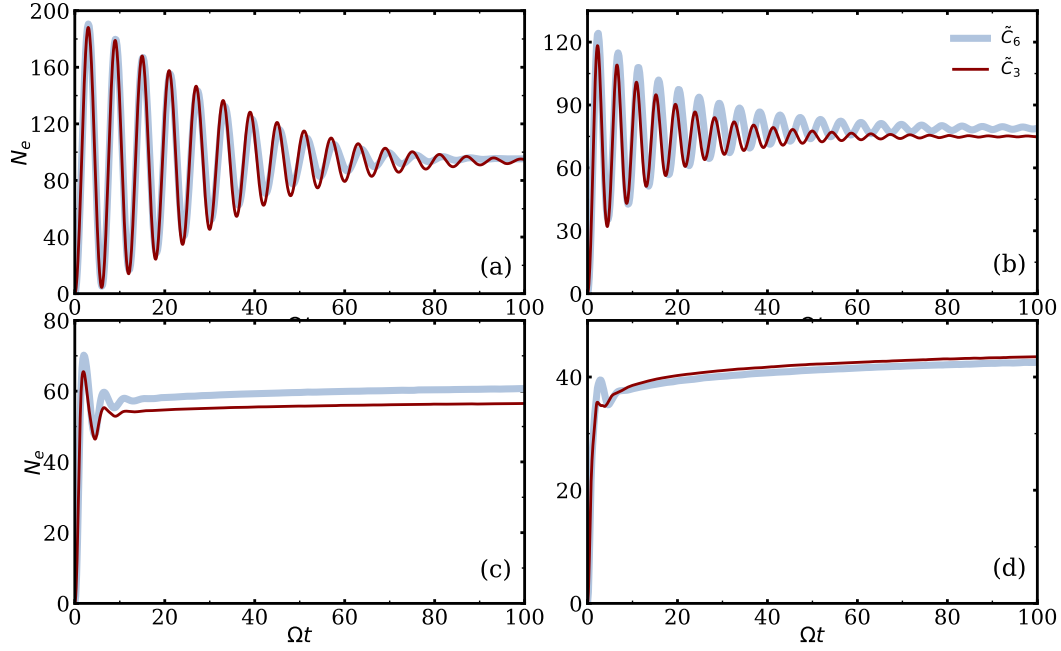


Figure 10. The dynamics of total number of excitations $N_e(t)$ in an atomic chain with $N = 200$, $\Delta = 0$ and for different \tilde{C}_6 and \tilde{C}_3 , using dTWA with the sampling schemes S_{III}. (a), (b) and (c) are respectively for $\tilde{C}_6 = \tilde{C}_3 = 0.2\Omega$, $\tilde{C}_6 = \tilde{C}_3 = \Omega$ and $\tilde{C}_6 = \tilde{C}_3 = 3\Omega$.

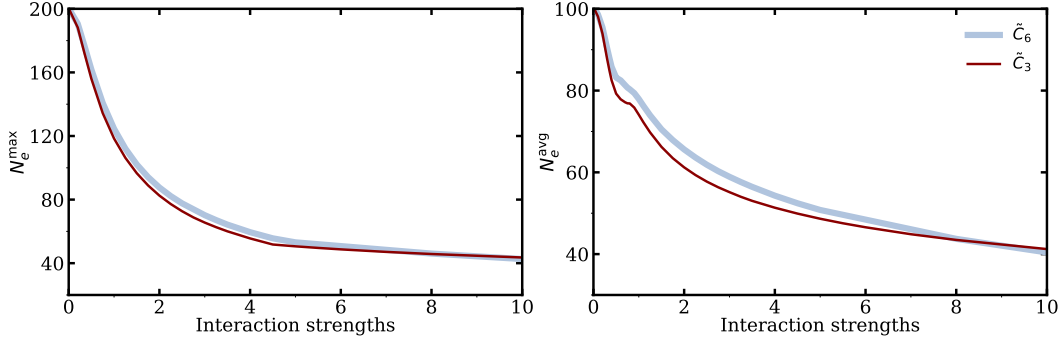


Figure 11. (a) The maximum (N_e^{max}) and (b) average (N_e^{avg}) number of excitations as a function of interaction strengths \tilde{C}_6 and \tilde{C}_3 , for $N = 200$ and $\Delta = 0$ using dTWA with sampling scheme S_{III}. For calculating N_e^{avg} , we took $\Omega T = 100$.

times disappear completely for large values of \tilde{C}_6 or \tilde{C}_3 . In figure 11, we show N_e^{max} and N_e^{avg} as a function of the interaction strengths, which exhibits similar behavior as of the $N = 10$ case.

7. Conclusions and Outlook

In conclusion, we have analyzed the excitation dynamics numerically in a chain of Rydberg atoms, interacting via either van der Waals or dipolar interactions via both

dTWA and ANN. For a small system, we compared the results with exact calculations, which helped us to outline the pros and cons of both approaches. Including the two-body correlations via BBGKY hierarchy in dTWA and increasing the number of hidden units, especially at large interaction strengths, are suffered by numerical instabilities. We see that dTWA can be easily extended to large systems, e.g., a system size of two hundred atoms compared to ANN. Future studies involve addressing the numerical instabilities in both dTWA-BBGKY and ANN and more accurately simulating long-time dynamics. It is also possible to extend the studies to multi-dimensional lattices and gas of Rydberg atoms in various dimensions. In particular, one would be interested in exploring many-body correlations, and the spatial patterns of the Rydberg excitations, including the dynamical crystallization [71].

8. Acknowledgments

We acknowledge UKIERI-UGC Thematic Partnership No. IND/CONT/G/16-17/73 UKIERI-UGC project. W.L further thanks the support from the EPSRC through Grant No. EP/R04340X/1 via the QuantERA project "ERyQSenS" and the Royal Society through the International Exchanges Cost Share award No. IEC\NSFC\181078.. R.N. further acknowledges DST-SERB for Swarnajayanti fellowship File No. SB/SJF/2020-21/19 and National Supercomputing Mission (NSM) for providing computing resources of 'PARAM Brahma' at IISER Pune, which is implemented by C-DAC and supported by the Ministry of Electronics and Information Technology (MeitY) and Department of Science and Technology (DST), Government of India. V.N. acknowledges the funding from DST India through an INSPIRE scholarship.

References

- [1] Czischek, S 2020 *Springer Theses*, Springer Nature Switzerland
- [2] Orús R 2014 *Ann. Phys.* **349** 117
- [3] White S R 1992 *Phys. Rev. Lett.* **69** 2863
- [4] Vidal G 2004 *Phys. Rev. Lett.* **93** 040502
- [5] Schollwöck U 2011 *Ann. Phys.* **326** 96
- [6] Bridgeman J C, Chubb C T 2017 *J. Phys. A: Math. Theor.* **50** 223001
- [7] White S R, Feiguin A E 2004 *Phys. Rev. Lett.* **93** 076401
- [8] Polkovnikov A 2010 *Ann. Phys.* **325** 1790
- [9] Blakie P B, Bradley A S, Davis M J, Ballagh R J, Gardiner C W 2008 *Adv. Phys.* **57** 363
- [10] Schachenmayer J, Pikovski A, Rey A M 2015 *New J. Phys.* **17** 065009
- [11] Schachenmayer J, Pikovski A, Rey A M 2015 *Phys. Rev. X* **5** 011022
- [12] Pucci L, Roy A, Kastner M 2016 *Phys Rev B* **93** 174302

- [13] Zhu B, Rey A M, Schachenmayer J 2019 *New J. Phys.* **21** 082001
- [14] Wurtz J, Polkovnikov A, Sels D 2018 *Ann. Phys.* **395** 341
- [15] Huber J, Rey A M and Rabl P arXiv:2105.00004
- [16] Khasseh R, Russomanno A, Schmitt M, Heyl M, and Fazio R 2020 *Phys. Rev. B* **102** 014303
- [17] Orioli A P, Signoles A, Wildhagen H, Günter G, Berges J, Whitlock S and Weidemüller M 2018 *Phys. Rev. Lett.* **120** 063601
- [18] Signoles A, Franz T, Alves R F, Gärttner M, Whitlock S, Zürn G and Weidemüller M 2021 *Phys. Rev. X* **11** 011011
- [19] Geier S et al arXiv:2105.01597
- [20] Hao L et al 2021 *New J. Phys.* **23** 083017
- [21] Lepoutre S, Schachenmayer J, Gabardos L, Zhu B, Naylor B, Maréchal E, Gorceix O, Rey A M, Vernac L and Laburthe-Tolra B 2019 *Nat. Commun.* **10** 1714
- [22] Fersterer P et al 2019 *Phys. Rev. A* **100** 033609
- [23] Patscheider A 2020 *Phys. Rev. Research* **2** 023050
- [24] Kunimi M, Nagao K, Goto S and Danshita I 2021 *Phys. Rev. Research* **3** 013060
- [25] Mehta P, Bukov M, Wang C-H, Day A G R, Richardson C, Fisher C K, Schwab D J 2019 *Phys. Rep.* **810** 1-124
- [26] Carleo G, Cirac I, Cranmer K, Daudet L, Schuld M, Tishby N, Vogt-Maranto L, Zdeborová L 2019 *Rev. Mod. Phys.* **91** 045002
- [27] Carleo G, and Troyer M 2017 *Science* **355** 602
- [28] Fabiani G, and Mentink J H 2019 *SciPost Phys.* **7** 004
- [29] Czischek S, Gärttner M, and Gasenzer T 2018 *Phys. Rev. B* **98** 024311
- [30] Wu Y, Duan L M, and Deng D L 2020 *Phys. Rev. B* **101** 214308
- [31] Deng D L, Li X, and Sarma S D 2017 *Phys. Rev. X* **7** 021021
- [32] Deng D L, Li X, and Sarma S D 2017 *Phys. Rev. B* **96** 195145
- [33] Deng D L 2018 *Phys. Rev. Lett.* **120** 240402
- [34] Browaeys A, and Lahaye T 2020 *Nat. Phys.* **16** 132
- [35] Bernien H, Schwartz S, Keesling A, Levine H, Omran A, Pichler H, Choi S, Zibrov A S, Endres M, Greiner M, Vuletić V, and Lukin M D 2017 *Nature* **551**, 579
- [36] Schlosser M, Ohl de Mello D, Schäffner D, Preuschoff T, Kohfahl L and Birkl G 2020 *J. Phys. B: At. Mol. Opt. Phys.* **53** 144001
- [37] Kim H, Park Y, Kim K, Sim H-S and Ahn J 2018 *Phys. Rev. Lett.* **120** 180502
- [38] Guardado-Sánchez E, Brown P T, Mitra D, Devakul T, Huse D A, Schauß P, and Bakr W S 2018 *Phys. Rev. X* **8** 021069
- [39] Labuhn H, Barredo D, Ravets S, De Léséleuc S, Macrì T, Lahaye T and Browaeys A 2016 *Nature* **534** 667

- [40] Graham T M, Kwon M, Grinkemeyer B, Marra Z, Jiang X, Lichtman M T, Sun Y, Ebert M, and Saffman M 2019 *Phys. Rev. Lett.* **123** 230501
- [41] Scholl P, Schuler M, Williams H J, Eberharter A A, Barredo D, Schymik K-N, Lienhard V, Henry L-P, Lang T C, Lahaye T, Läuchli A M, and Browaeys A arXiv:2012.12268
- [42] Ebadi S, Wang T T, Levine H, Keesling A, Semeghini G, Omran A, Bluvstein D, Samajdar R, Pichler H, Ho W W, Choi S, Sachdev S, Greiner M, Vuletić V, and Lukin M D, arXiv:2012.12281.
- [43] Bluvstein D, Omran A, Levine H, Keesling A, Semeghini G, Ebadi S, Wang T T, Michailidis A A, Maskara N, Ho W W, Choi S, Serbyn M, Greiner M, Vuletić V, and Lukin M D, 2021 *Science* **371** 1355
- [44] Saffman M, Walker T G, and Mølmer K 2010 *Rev. Mod. Phys.* **82** 2313
- [45] Béguin L, Vernier A, Chicireanu R, Lahaye T and Browaeys A 2013 *Phys. Rev. Lett.* **110** 263201
- [46] Lukin M D, Fleischhauer M, Cote R, Duan L M, Jaksch D, Cirac J I. and Zoller P 2001 *Phys. Rev. Lett.* **87** 037901
- [47] Gaëtan A, Miroshnychenko Y, Wilk T, Chotia A, Viteau M, Comparat D, Pillet P, Browaeys A and Grangier P 2009 *Nat. Phys.* **5** 115
- [48] Urban E, Johnson T A, Henage T, Isenhower L, Yavuz D D, Walker T G and Saffman M 2009 *Nature Physics* **5** 110
- [49] Weimer H, Müller M, Lesanovsky I., Zoller P and Büchler H P 2010 *Nat. Phys.* **6** 382
- [50] Schauß P, Cheneau M, Endres M, Fukuhara T, Hild S, Omran A, Pohl T, Gross C, Kuhr S and Bloch I 2012 *Nature* **491** 87
- [51] Barredo D, Labuhn H, Ravets S, Lahaye T, Browaeys A and Adams C S 2015 *Phys. Rev. Lett.* **114** 113002
- [52] Zeiher J, Van Bijnen R, Schauß P, Hild S, Choi J Y, Pohl T, Bloch I and Gross C 2016 *Nat. Phys.* **12** 1095
- [53] Zeiher J, Choi J Y, Rubio-Abadal A, Pohl T, van Bijnen R, Bloch I and Gross, C 2017 *Phys. Rev. X* **7** 041063
- [54] Marcuzzi M, Minář J C V, Barredo D, de Léséleuc S, Labuhn H, Lahaye T, Browaeys A, Levi E and Lesanovsky I 2017 *Phys. Rev. Lett.* **118** 063606
- [55] Gross C and Bloch I 2017 *Science* **357** 995
- [56] Jaksch D, Cirac J I, Zoller P, Rolston S L, Côté R and Lukin M D 2000 *Phys. Rev. Lett.* **85** 2208
- [57] Wilk T, Gaëtan A, Evellin C, Wolters J, Miroshnychenko Y, Grangier P and Browaeys A 2010 *Phys. Rev. Lett.* **104** 010502
- [58] Isenhower L, Urban E, Zhang X L, Gill A T, Henage T, Johnson T A, Walker T G and Saffman M 2010 *Phys. Rev. Lett.* **104** 010503

- [59] Saffman M 2016 *J. Phys. B: At. Mol. Opt. Phys.* **49** 202001
- [60] Su S.-L., Guo F.-Q., Wu J.-L. , Jin Z, Shao X Q, and Zhang S 2020 *Europhys. Lett.* **131**, 53001
- [61] Basak S, Chougale Y, and Nath R 2018 *Phys. Rev. Lett.* **120** 123204
- [62] Glaetzle A W, Nath R, Zhao B, Pupillo G, and Zoller P 2012 *Phys. Rev. A* **86** 043403
- [63] Wootters W K 1987 *Ann. Phys.* **176** 1
- [64] Wootters W K 2003 *arXiv:quant-ph/0306135*
- [65] Sorella S 2001 *Phys. Rev. B* **64** 024512
- [66] Neuscamman E, Umrigar C and Chan G K 2012 *Phys. Rev. B* **85** 045103
- [67] Hofmann D, Fabiani G, Mentink J H, Carleo G and Sentef M A arXiv:2105.01054
- [68] Wu G, Kurz M, Liebchen B, and Schmelcher P 2015 *Phys. Lett. A* **379** 143
- [69] Eberly J H, Narozhny N B, and Sanchez-Mondragon J J 1980 *Phys. Rev. Lett.* **44** 1323
- [70] Rempe G, Herbert W, and Klein N 1987 *Phys. Rev. Lett.* **58** 353
- [71] Pohl T, Demler E, Lukin M D 2010 *Phys. Rev. Lett.* **104** 043002